Journal of Thermal Analysis and Calorimetry, Vol. 86 (2006) 2, 521–529

IDENTIFICATION OF MICRO-SCALE CALORIMETRIC DEVICES
Part V. Basic properties for gas–solid reactions

C. Auguet[1], *J. L. Seguin*[2], *F. Martorell*[1], *F. Moll*[3], *V. Torra*[1*] *and J. Lerchner*[4]

[1]CIRG-DFA-ETSECCPB, Polytechnical University of Catalonia, Campus Nord B-4, 08034 Barcelona, Catalonia, Spain
[2] Laboratoire Matériaux et Microélectronique de Provence (L2MP, UMR 6137 CNRS), Université d'Aix-Marseille III Faculté des Sciences et Techniques de St. Jérôme, case 152, 13397 Marseille Cedex 20, France
[3]DEE, Polytechnical University of Catalonia, C/Gran Capità s/n, Campus Nord C-3, 08034 Barcelona, Catalonia, Spain
[4]Institut f. Physikalische Chemie, TU Bergakademie Freiberg, Leipziguer Str. 29, 09596 Freiberg/Sachsen, Germany

Micro-calorimetric devices using Si-based sensors are very useful for the study of gas–solid reactions, in which very low mass of reactants are necessary. But in fact the consequence of using flat detectors is an increase of the uncertainty in the measured energy. In this work a calorimetric gas sensor based on Xensor chip is analysed studying the local *x–y* contributions of dissipation to the sensitivity related to the value in the centre. We study also the effects of the gas-flow on the sensitivity, comparing the results obtained with two Xensor type chips. Finally we carry out a deeper analysis of the *x–y* effects on the calorimetric detector for dissipations in the reactant shell extremely close to the detector surface to visualize the link between the power density distribution and the output signal.

Keywords: *accuracy, chemical nose, conduction calorimeters, gas–solid detectors, position effects*

Introduction

Gas–solid reactions relate one of the most important research subjects in sensors-actuators systems. Several specific sensors are described in the recent literature [1]. In fact, arrays of different sensors are in the basis of the chemical (or electronic) nose [2]. Mainly conductometric sensors (metal oxide, ionic conductor or conductive polymer) and quartz microbalances are used. Also it has been shown that integrated circuit microcalorimeters coated with a gas sensitive film can be applied for gas detection [3, 4]. The calorimetric improvements are related to 'reactions' between extremely lower masses [5, 6]. For instance, in analytical studies the actual target is situated close to several μg for mass of the reactants. Development of the calorimetric devices and the need of improved results for these lower masses induces two levels of difficulties: The first one is the use of highly sensitive elements as the Al–Si [7] thermocouples and appropriate auxiliary elements (i.e., pumps and temperature control) and the second one relates an improved outline of the devices and of the heat transfer formalism. In fact, the main target of this and previous papers I, II, III and IV [8–11] is the analysis of 'calorimetric' devices for improved quantitative results. By other hand, geometrical problems can also decrease the reability of calorimetric results [12].

The last, but not the least, relates the particular characteristics of the studied phenomena: liquid–liquid mixture, the gas–solid reaction, and so on. The former mainly requires the analysis of the steady state situation but the later is usually associated to transitory situations with increased difficulties in the formalisms.

Some qualitative and introductory observations are outlined. By one hand, two standard manufactured nano-calorimetric devices using two Xensor detectors are used to analyse the sorption process of gaseous guest compounds onto sensor coatings. By other hand, simultaneous measurements associated to gas–solid reaction via a resistive gas sensor.

Gas–solid reactions in the field of solid-state gas sensors

Gas–solid reactions are the basis of many solid-state gas sensors which are mainly of resistive type. Solid-state resistive gas sensors may be based on bulk conduction or surface layer conduction. In the first case, gas–solid reactions modify the bulk stoichiometry which results in a bulk conductivity change. This principle has been applied to oxygen sensors for automotive exhaust. With the surface layer conduction, surface reaction with the gases modifies the concentration of the mobile electrical charges, which change the conductivity. The bulk conduction sensors are limited to the oxygen measurement and the response time is often slower, due to the stoichiometry

* Author for correspondence: torra@fa.upc.es

1388–6150/$20.00
© 2006 Akadémiai Kiadó, Budapest
Akadémiai Kiadó, Budapest, Hungary
Springer, Dordrecht, The Netherlands

change which is related to a diffusion mechanism [13]. So, thin or thick films sensors based on a change of the surface conduction are preferred to the bulk ones. Moreover they allow better on-chip integration and mass-production, and are often cheapest.

Copper(I) bromide ammonia sensor is an example of how a specific gas–solid reaction can be used to implement a highly selective gas sensor. Copper(I) bromide CuBr is used for ammonia gas sensing, based on the reported existence of very stable Cu^+–ammonia complexes in aqueous solution, such as $[Cu(NH_3)_2]^+$. This mixed conductor shows large Cu^+ ion mobility and a modest electron hole conductivity of CuBr at ambient temperature. CuBr films can be prepared by magnetron sputtering [14, 15], but most efficiently by chemical reaction between Cu metal and an aqueous $CuBr_2$ solution [16]. Prior to use as sensor, the films must be conditioned few hours under an ammonia partial pressure of 100 mbar. This initial treatment is necessary to stabilize the films and get reproducible and long-time stable measurements. After the first exposure to a high ammonia concentration, the sensors are kept at ambient atmosphere. The sensor effect can be interpreted by a two-step mechanism:

- A monolayer of chemisorbed NH_3 molecules is formed at the CuBr surface with Cu^+ ions attracted to the surface during the initial ammonia treatment. The copper ion vacancy concentration is enhanced in negatively charged space charge regions that counterbalance the positive surface charge. These regions very easily percolate through the samples. They represent high conductivity regions, short-circuiting the bulk and strongly enhancing the film conductivity after the initial ammonia treatment.
- After formation of a chemisorbed ammonia monolayer, further ammonia molecules are physisorbed during the sensor measurements. Physisorption relies on weak Van der Waals forces: the observed small decrease of the bulk conductivity may be attributed to dipolar effects (reduction of electron hole mobility). This step is totally recoverable and the initial conductivity is found after the ammonia gas stream is switched off.

A typical dependence of the electrical resistance of CuBr films on the ammonia partial pressure in the gas phase, at room temperature, is shown in Fig. 1.

A quantifying process between the resistance measurements and the energetic dissipation, requires tentative measurements determining an approach to working scales previous to some considerable effort need for building an improved calorimetric device inside the 'open chamber' used in surface analysis studies.

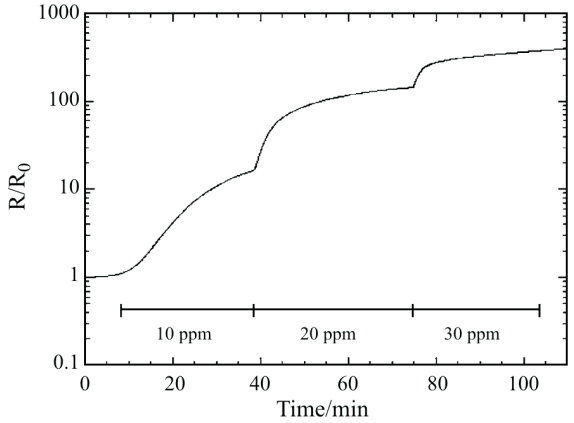

Fig. 1 Resistance variation *vs*. time for a sputtered CuBr film with interdigitated copper electrodes, exposed to small step-varying concentrations of NH_3 at room temperature (gas flow: 24 L h^{-1}, applied dc voltage: 100 mV). R_0 is the resistance in pure air

Calorimetric detection of gas solid reactions

In the case of energetic measurements the experimental system used was constructed using two Xensor LCM 2524 nano-calorimeter sensors [17]. The experimental device permits the simultaneous detection of the two signals produced by the same gas acting on two different polymers. The supply of the sample gas (synthetic air plus 'guest' gas) and of the reference gas (only synthetic air) is provided through tubes with labyrinth path inside a metallic element to ensure a homogeneous temperature. Each detector uses a half of the total gas flow. The experiment consists in measuring the absorption enthalpy in the solid–gas interaction when the sample gas reacts with the polymer, and the corresponding to degassing (or desorption enthalpy) when only the pure reference gas is used. From thermodynamic point of view two well definite states are necessary; i.e., completely degassed state ('infinite' time of degassing), and well defined time of reaction with known concentration.

For analyzing the heat loss by the flowing gas the following experiments were performed [18]:

- Measuring steady state Joule effects due to chip heater at constant heat power and different volume flow rate and different polymer thickness.
- Measuring the integral effects for the absorption and desorption of heptane for the given polymer at different flow rate, different polymer thickness and at fixed sample concentrations.
- Analyzing the nozzle direction effects by steady state Joule heating and absorption experiments at fixed flow rates and polymer layers but with different nozzle designs.

In the experiments series of transient heat power pulses are produced by periodical excitation of the

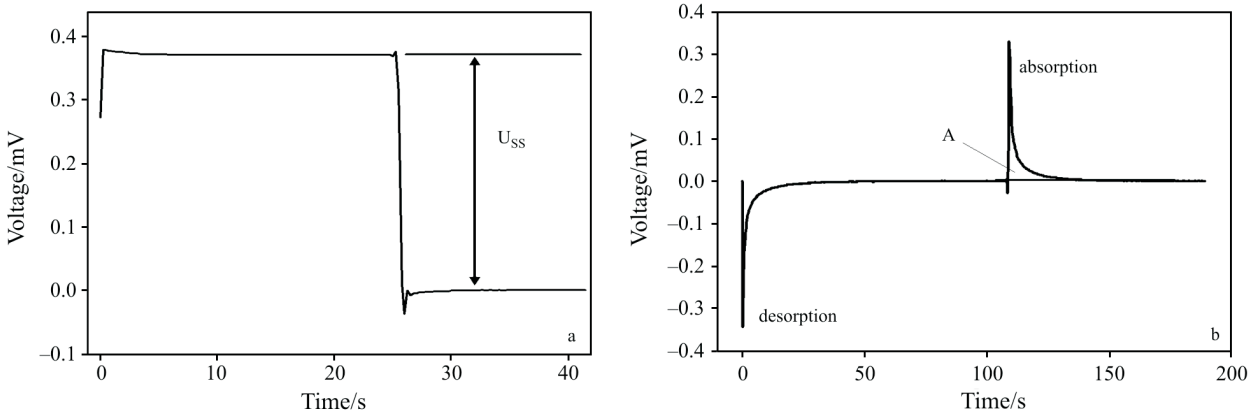

Fig. 2 Averaged signals of a – periodical Joule heating and b – heptane absorption–desorption series. U_{ss} – steady-signal for Joule heating power of 149 μW; A – peak area of the absorption of heptane on PDMS at 1000 ppm

Joule heater and by switching the gas flow between pure synthetic air and a mixture containing heptane gas, respectively. Figure 2 depicts the averaged curves of 30 periods for Joule heating as well for heptane absorption–desorption series. The signals of the Joule heating steady-state signals U_{ss} and the peak areas A corresponding to the heptane absorption were derived from averaged curves.

Actual detectors in calorimetric gas–solid work

The actual detectors, usually flat, only cover a practically 'zero part' of the whole surface enclosing the reaction volume. Also, in some calorimetric sensors, the detector direction is practically orthogonal to the heat flux. The consequence is an increased uncertainty in the measured energy. The devices furnish reproducible results with an increased uncertainty in the systematic error level. The systematic errors are less relevant for selection of reactive substances as than for thermochemical one when enthalpy values are of critical interest.

In this work a calorimetric gas sensor based on Xensor chips is analysed at three levels. Firstly, the local positioning effects in static situations applying a laser beam onto chip surface, as much as his parasitic laser effects, to ensure appropriate contributions of local (*x*–*y*) dissipation to the sensitivity related to the value in the centre. Secondly, we analyse the roughly effects of gas flow on the sensitivity, and we compare the results using two Xensor type chips. The last part includes some deep analysis about the *x*–*y* effects on the calorimetric detector, in particular for dissipations in the reactant shell extremely close to the detector surface. The analysis visualizes the link between the power density distribution and the output signal. The main target relates the effects associated to localized inhomogenities in the surface dissipations.

Calorimetric devices

The positional *x*–*y* analysis is realized via a laser signal (spot surface close to 1 mm^2) that impinges normally on the flat silicon surface of the LCM 2524 Xensor chip. This chip consists of large mono-crystalline silicon membrane 25 μm thick, 8·8 mm^2, in a thick silicon rim. The sensitive area in the middle of the membrane contains a diffused (*p*-type silicon) resistor heater integrated in the membrane. It is a square torus of 3.5·3.5 mm size and about 50 μm wide. Some analysis is realized using the NCM 9924 Xensor Chip (40 μm thick). It has, among of a diffused (*p*-type silicon) resistor heater integrated in the membrane in the same way than in the LCM 2524 chip, two aluminium meander resistances, galvanically isolated from the thermopiles, on the rear part of the surface. One of them is square torus of 3.8·3.8 mm^2, and about 50 μm wide, underneath the chip heater, and the other is 2.6·2.65 mm^2 squared shape, nearly centred [7].

A scheme of the system is well described in reference [8]. Laser light furnishes only a relatively appropriate tool: the photoelectric effect induces highly relevant actions in the output signal. The photon-electron signal, positive or negative and position dependent, overcomes 150 mV. The thermal signal induced by the same laser spot remains under 2.5 mV. In Fig. 3a the position of chip thermopairs and heater resistor on the chip is schematized. In Fig. 3b the positional effect of the photon-electron signal is shown.

To avoid the photoelectric effect an electronic gate makes the digitizing process starts 1 ms after the power shutdown on the laser beam, and the DMM reads the calorimetric decay signal when the photoelectric effect is completely disappeared. To facilitate the readability of the relative slow measurements the output signal is digitized (1024 samples) via a DMM Keithley 2000 multimeter. The sampling is close to 0.0113 s. To smooth the 50 Hz ripple, a mean of 12 signals is used.

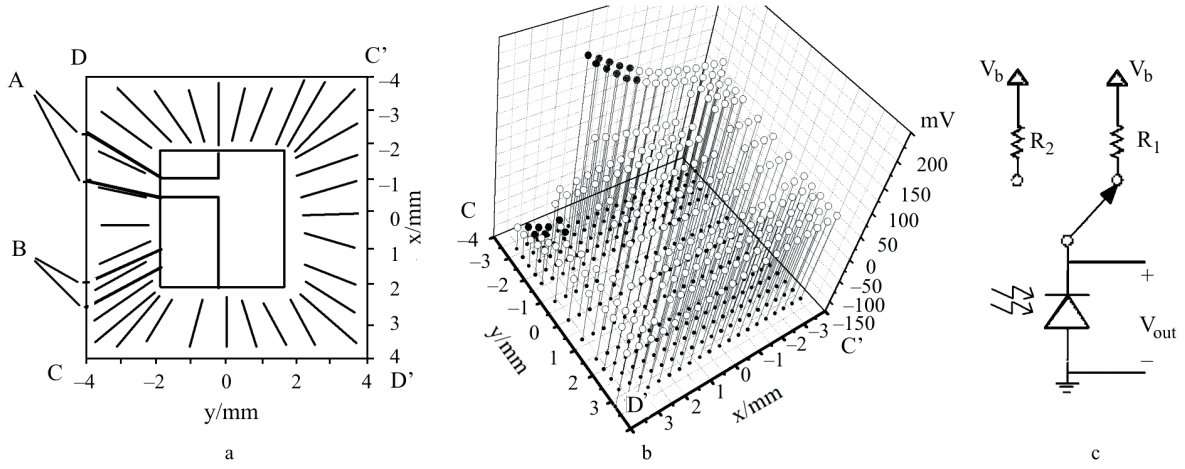

Fig. 3 a – Scheme of the chip with the thermo pairs and the squared heater (view from upper part of chip). A indicates the external heater links. B indicates the external thermo pairs links. C, C', D and D' indicate a roughly approach of the correspondence with the position of photon electron signal (see center). b – Photon-electron signal produced by the laser over the chip LCM 2524 surface. c – Scheme of the photodiode circuit

As a complementary idea, we checked if absorption light by Si-surface is the same in the central (work) zone (chip LCM 2524) than in the thermopairs zone. For this we made a rough evaluation of the transmitted and reflected light with an elementary system. We used a photodiode, which received the direct beam, the transmitted or the reflected light. The transmission signal has been measured with a distance of 9.5 cm from the laser to the chip, and 5 cm from the chip to the photodiode, with normal incidence. The output signal is digitized via the DMM Keithley 2000 in the same way than for the *x*–*y* positional study.

A scheme of the used circuit is shown in Fig. 3c. It consists of a photodiode (Siemens BPW34, with a maximum response at 900 nm) reversibly biased with a resistor *R* to a fixed voltage, V_b. When no light is incident on the photodiode surface, the current is negligible, and therefore the measured output voltage is the applied bias voltage, V_b. When the light impinges on the photodiode surface, a reverse current appears which is proportional to the light intensity [19].

In this case, the output voltage is $V_{out}=V_b-\alpha IR$, being *I* light intensity, α the photodiode response, *R* the resistance and V_b the applied voltage. Two possible values of resistance can be alternatively selected to get two different sensitivity values and obtain a signal proportional to the light intensity (i.e. using the direct signal and the transmitted signal).

Finally, for preliminary and roughly gas flow rate experiments we injected CO_2 over the centre of the chip surface with two incidence angles, 45 and 90º, keeping the nozzle at a distance of 5 mm over the chip centre. The nozzle hole diameter is 5 mm. The system is roughly protected of external air flows. To regulate the flow rate we used an ABB rotametre calibrated for working at 293 K, with nominal flow rates for N_2 gas between 0 and 1.27 $cm^3\ s^{-1}$ at the atmospheric pressure, and for CO_2 gas between 0 and 1.33 $cm^3\ s^{-1}$ in the same conditions. In our analysis we used flow rates for the CO_2 between 0 and 0.4 $cm^3\ s^{-1}$ at the atmospheric pressure, and the laboratory temperature (air conditioned) is close to 293 K.

Positional effects in static situation: *x*–*y* detailed analysis by laser

The dissipated heat by the laser in the flat surface shows a clear dependence [8] from the center to the external boundaries. Figure 4a shows the detailed analysis of sensitivity values in reduced units (it means, divided by the sensitivity value of the central point), as the power absorbed by the laser is unknown, on the chip surface. The results relate a Xensor LCM 2524 Si-based device without parasitic photoelectric effects [8, 20]. The standard deviation for the signal value of each experimental point is about ±1%. A progressive displacement of dissipated heat from the center to the external boundary acts, firstly, in the warm junctions and moves, progressively, to cold junctions. In fact, negative values can be, also, measured in the boundaries of the Si-surface (dissipation near the cold junctions of thermopairs). It is possible to see that in central work surface of 2·2 mm^2 the peak to peak fluctuation of sensitivity values reaches the 9% (in corner D, Fig. 4b, and considering the central work surface of 4·4 mm^2, the 40% (in corner D, Fig. 4c). The geometrical diagonal distribution CC' and DD' are the same in Figs 3a and b and also in Fig. 4.

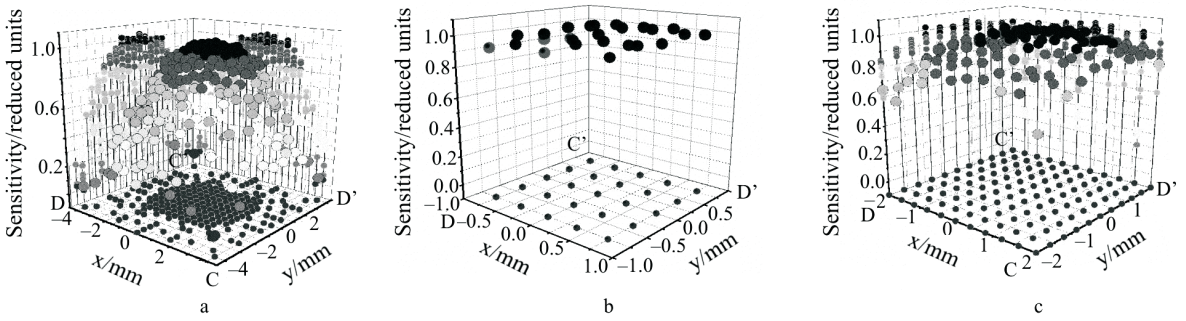

Fig. 4 Sensitivity in reduced units *vs*. *x*–*y* position. a – For all points distributed in the available (8·8 mm^2) Si surface. Projections on the planes *x*–*z* and *y*–*z* are also visible. b – For the central part of the Si surface, 2·2 mm^2. c – For the useable surface inside 'warm' junctions (central part of the Si surface, 4·4 mm^2). It is shown the decrease of sensitivity value from the center to the extreme. The asymmetry along DD' diagonal is stronger than along the CC' diagonal

Due to the causal fluctuation in the inner space, the mean sensitivity should be calculated over the complete working surface of the chip as

$$\bar{S} = \frac{1}{A}\iint_{A} S(x, y)\mathrm{d}x\mathrm{d}y \qquad (1)$$

The mean value of sensitivity decreases quickly as it is calculated for bigger inner work areas, as it is shown in Table 1, for chips 963 and 964.

Table 1 Mean sensitivity values (in reduced units, it means, divided by the value of the sensitivity in the central point) for different central work areas (in mm^2). The area of 5.76 mm^2 corresponds to a squared frame of side 4 and 0.36 mm wide as indicated in Fig. 7c

Area/ mm^2	Mean sensitivity		
	reduced units	V/W Chip 963	V/W Chip 964
1	0.99	1.27	1.24
4	0.96	1.23	1.21
9	0.94	1.21	1.18
16	0.90	1.15	1.15
5.76	0.83	1.06	1.04

These results indicate that using the central part of the available surface (4·4 mm^2), manufactured as the recommendable working surface, relates a decrease of sensitivity of 10%. This decrease is somewhat stronger than found in a previous analysis where a more roughly methodology was applied [20].

For each surface dissipation a shape factor can be defined [20] from the ratio between the sensitivity in the surface related with the actual dissipation and the sensitivity in the surface occupied by the chip heater (furnished by the manufacturer). For each configuration it is possible to find a shape factor F_{xyz} such as the effective sensitivity should be calculated as $S_{ef}=F_{xyz}S_J$, being S_J the sensitivity obtained via Joule heating using the chip heater.

Analyzing the *x* and *y* coordinates by heat transfer models, the sensitivity behavior shows some squared symmetry related to the particular shape of the detectors. The experimental scatter avoids any visualization of the squared symmetry. A detailed analysis of the results in Fig. 4c clearly shows an asymmetry along the diagonal DD', which is stronger than along the CC' diagonal: the sensitivity decreases in the neighborhood of the external heater links (Fig. 3a). This asymmetrical behavior does not seem related to residual photoelectric effects: the non-symmetry in DD' (Fig. 4c) cannot match with some growing spiral (full dots in Fig. 3b).

Laser parasitic effects of transmission, absorption and reflection of laser light

The transmission signal has been measured placing consecutively the chip at a distance of 9.5 cm from the laser, and 5 cm from chip to the photodiode, with normal incidence and using low sensitivity (low resistance value) as indicated below. We analysed the transmission values in a wide number of points of the chip from the centre to the surroundings, realising a mean of 15 measurements in each case. The obtained signal values decrease from 0.73±0.03 mV in the centre up to 0.65±0.02 mV for C and C' corners, 0.69±0.02 mV in the corner D, and 0.53±0.03 mV in the D' one. The distribution of transmitted light shows again some asymmetric behaviour along the DD'.

By other hand, comparing these values with the signal obtained applying the laser directly to the photodiode, which is 2.771±0.006 V, we can see that the transmitted light is extremely low. Also we have made measurements of reflection in two chips, from which we have obtained more uniform values of signal for the same different positions over the chip surface.

The non-symmetric behaviour in the transmission can be associated to the inhomogeneous rear part of chip by different absorption/reflection associated

to heater and thermo-pairs. At the practical level the different absorption effect are irrelevant in comparison with the sensitivity changes in the chip, it means, the absorbed power in Si-surface of NCM chip seems more homogeneous due to the presence of aluminium heaters in all of the rear part.

Gas flow effects in sensitivity

In order to clarify the effects of the variations of local sensitivity with flow rate, we studied the behaviour of chip response when a gas flow overcome on the chip surface with different flow rates and for different power in the chip resistance. The procedure has been as follows: we start recording the zero chip signal, then start the gas injection holding a constant flow rate with normal incidence. Flow rates between 0 and 0.4 cm^3 s^{-1} were used. When stationary state is achieved, different power values are dissipated, nearly between 0.1 and 1.1 mW. We return to the zero power value every time. An example of the recorded signal obtained with this procedure is shown in Fig. 5.

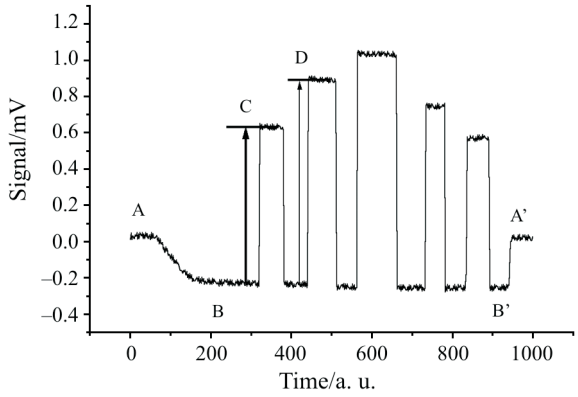

Fig. 5 Calorimetric output obtained changing the dissipated power (C, D) at constant flow rate. AA' is the baseline without flow gas nor dissipated power. BB' is the baseline at constant flow rate, without dissipated power

The sensitivity obtained is referenced to the base line corresponding to zero power and constant gas flow rate (BB' line in Fig. 5). We can see in Fig. 6a that the sensitivity decreases as the power increases, and only a lower decrease is detected with the increasing flow rate. The experimental analysis suggest that in chip LCM 2524 it exists a non-linearity produced by the dissipated power in the chip heater. The measurements uses battery power supply completely isolated from the output but eventually parasitic cross-talk effects between heater and thermopile cannot be completely avoided. The behaviour of the sensitivity against power dissipation for an incidence angle of roughly 45º is similar than for normal incidence.

We repeated the same experiment with the NCM 9924 chip. To use the central aluminium resistance for power dissipation means that the dissipation is made in a more extent and uniform part of the surface (6.89 mm^2 in comparison with 0.7 mm^2) and by other hand the heat transfer acts on a higher silicon thick than in the case of the LCM 2524 (40 *vs.* 25 μm). Increased surface and thickness works in the appropriate direction. This fact implies a more realistic approach to the energetic dissipation that would take place in a reaction between an incident gas over a deposited substance on the surface. By other hand, it is still not equivalent to a real situation because the reactive substance would be placed on the upper part of the chip surface when the aluminium resistance is placed on the rear part of it.

We have measured the signal using by one hand the heater resistor, and by other hand the aluminium resistance placed in the centre, following the same procedure as with the former chip. Figure 6a and b shows the power dependence for the LCM 2524 and for the NCM 9924 respectively. It is possible to appreciate the disappearance of the previous non-linearity.

We studied two different chips NCM 9924 type. The results for the mean sensitivity using the chip heater or the aluminium heater are shown in Table 2.

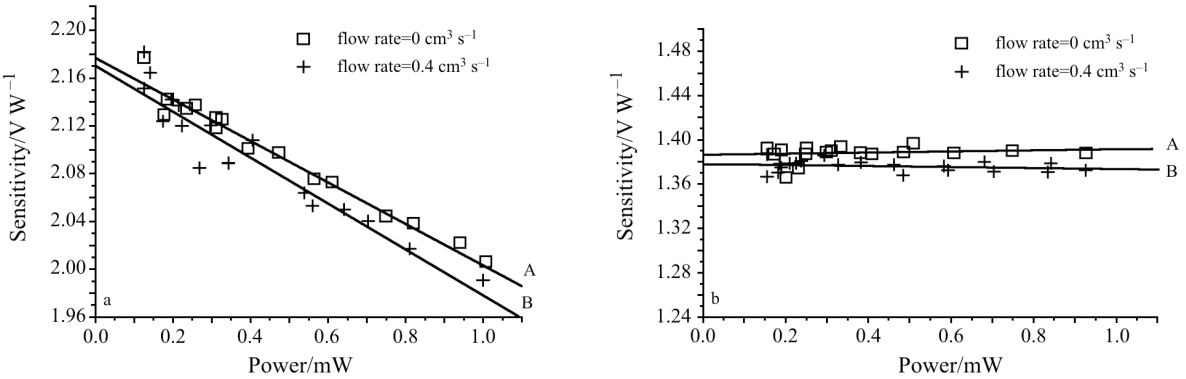

Fig. 6 Sensitivity *vs*. the dissipated power for constant gas flow rates. A and B are the linear fit for both series of experimental points. a – Power dissipation in the chip heater of the LCM 2524 Xensor chip. b – Power dissipation in the central aluminium resistance of the NCM 9924 Xensor chip

Table 2 Positional effects in furnished resistances for NCM 9924 type Xensor chips. Mean sensitivity in V/W

	Chip heater	Al heater
Chip 963	1.3823±0.0062	1.4053±0.0037
Chip 964	1.3575±0.0032	1.3707±0.0061

Upper level resistance films (silver)

The positional effect of sensitivity from the laser on the surface is known in reduced units as indicated previously. Assuming a homogeneous power dissipation in the aluminium heater on a NCM9924 Xensor type chip, it is possible to find a coefficient f_a which will be used to convert the relative sensitivity (in reduced units) to absolute sensitivity (in V W^{-1}). To show this, we found this factor as we show below, and we used it to calculate the signal obtained from a thin film of Ag resistance on the work surface of a chip, as shown in Fig. 7a, and we compared the result with the experimentally measured signal.

We can assume a homogeneous power dissipation in the aluminium heater, it means, the dissipated surface power density can be considered constant. The location of the aluminium heater in the chip is well determined, and we have measured the signal s_{Al} obtained from the Al heater for different given power. Then we can assign the laser sensitivity in reduced units, obtained for each position of a grid surface, to calculate the factor f_a from the expression connecting the local dissipation with the output signal (linearity is assumed):

$$s_{Al} = \sum_i s_{i,Al} = f_a \sum_i A_0 w S_i = f_a A_0 w \sum_i S_i \quad [V] \quad (2)$$

where $s_{i,Al}$ are the elementary signals related with each surface element, $w=W/A$ (W mm^{-2}) is the dissipated power surface density, assumed constant, W is the dissipated power on the aluminium heater and A is his area. A_0 is the area, in mm^2, of the elemental square unit of the grid positions corresponding to the places where the laser dissipation were measured. S_i is the laser sensitivity in reduced units for each elemental position associated to each squared unit A_0. The factor f_a can be obtained as

$$f_a = \frac{s_{Al}}{A_0 w \sum_i S_i} \quad [V\ W^{-1}] \quad (3)$$

This factor establishes the link between the sensitivity associated to the chip surface obtained from the laser measurements, in reduced units, and the absolute sensitivity in V W^{-1}. It means that we can estimate what will be the measured signal from a dissipation made on the surface using a film of Ag resistance, in which we assume that the new surface power density w' is also constant, and that the dissipation in upper or in the bottom surfaces do not changes the result in relevant effect.

Then, applying again the same previous laser grid of positions to identify the sites of dissipation, we can estimate the value s_{Ag} of calculated signal using the obtained factor f_a, and considering the Ag heater roughly divided in j parallel bands, each one with i unit elements distributed from one wire to the other, as indicated in Fig. 7b

$$s_{Ag} = f_a A_0 \sum_{ij} w'_{ij} S_{ij} \quad [V] \quad (4)$$

where w'_{ij} is the surface power density dissipated in each band j with N_j elements of area A_0. S_{ij} is the laser sensitivity, in reduced units, measured for the ij element.

If we consider that the voltage V is applied over a system of roughly parallel resistances formed by j bands, each one with N_j elements, as it is shown in Fig. 7b, and assuming that the dissipated power is constant for each band, the intensity due to the applied voltage in one band j with N_j elements reads:

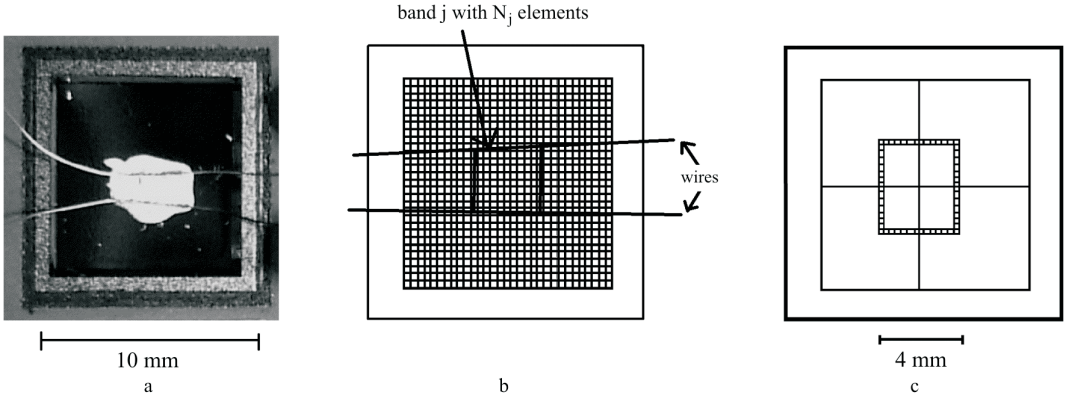

Fig. 7 a – Picture of chip Xensor NCM 9924 number 963, with a film of Ag on the surface and the wires which the voltage is applied. b – Band resistances (schematic) in which it is considered divided the Ag heater using the laser grid positions. Each element ij has an elemental resistance of value R_0. c – Scheme of squared frame of side 4 and 0.36 mm wide

Table 3 Examples of data for the calculus of measured signal obtained in Ag thin layer from the factor f_a for two chips Xensor NCM 9924 type. W: dissipation in Al heater. W_{Ag}: dissipation in Ag film

Chip number 963								
W/W	s_{Al}/V	f_a/V W^{-1}	W_{Ag}/W	V/V	R_0/Ω	Calculated s_{Ag}/V	Measured s_{Ag}/V	Difference/%
0.8684e-3	1.219e-3	1.281	0.8966e-3	0.0236	1.657	1.109e-3	1.107e-3	0.2
1.0269e-3	1.444e-3	1.283	1.0279e-3	0.0253	1.661	1.274e-3	1.266e-3	0.6
Chip number 964								
W/W	s_{Al}/V	f_a/V W^{-1}	W_{Ag}/W	V/V	R_0/Ω	Calculated s_{Ag}/V	Measured s_{Ag}/V	Difference/%
0.6096e-3	0.837e-3	1.253	0.6400e-3	0.0829	24.90	6.906e-4	6.961e-4	0.8
0.7392e-3	1.075e-3	1.259	0.7310e-3	0.0885	24.85	7.924e-4	7.964e-4	0.5

$$I_j = \frac{V}{R_j} = \frac{V}{R_0 N_j} \quad \text{[A]} \quad (5)$$

where R_j is the resistance of the band j and R_0 is the resistance of each element. The dissipated power in one element

$$W_{ij} = \frac{VI_j}{N_j} = \frac{V^2}{R_0 N_j^2} \quad \text{[W]} \quad (6)$$

It means, the signal produced by one element ij reads:

$$s_{ij} = f_a \frac{V^2}{R_0 N_j^2} S_{ij} \quad \text{[V]} \quad (7)$$

The signal for one band reads:

$$s_j = \sum s_{ij} = f_a \frac{V^2}{R_0 N_j^2} \sum_i S_{ij} \quad \text{[V]} \quad (8)$$

and the calculated signal from the Ag heater, it means, the total signal for the j bands

$$s_{Ag} = f_a \frac{V^2}{R_0} \sum_j \sum_i \frac{S_{ij}}{N_j^2} \quad \text{[V]} \quad (9)$$

where V is the applied voltage over the Ag heater, R_0 is the value of the resistance for each ij element, and it must be found assuming that the total resistance is equivalent to a parallel system of j bands having each one N_j elements such as

$$R_0 = \frac{V^2}{W_{Ag}} \sum_j \frac{1}{N_j} \quad [\Omega] \quad (10)$$

where W_{Ag} is the total dissipated power in the Ag film. Equation (9) with (10) can be formulated in terms of the shape factor formalism established in [8, 20].

We applied this roughly approach to two NCM 9924 chips and we compared the obtained results with the measured ones. We obtained that for all dissipated power between 0.5 and 1.2 mW the relative error between measured and calculated signal is less than 1%. Some results can be seen in Table 3.

In this way, it is possible to assign to each element of the chip surface a sensitivity in V W^{-1} multiplying the corresponding laser sensitivity (in reduced units) by the obtained factor f_a (in V W^{-1}) for each chip. The results are shown in Table 1 for both studied chips. The analysis suggests that the positional sensitivity established by laser measurements can be converted to 'absolute units' via Joule effects with an uncertainty close to 1% in the central area. Also, the measurements suggest the possibility of more complex analysis related to the positional effects in the reaction. (i.e., using different w_{ij} for each surface element).

Conclusions

The experimental analysis establishes relevant differences in the heat dissipation position related to poor heat flux integration. Improved accuracy needs supplementary adapted hypothesis and experimental measurements. For gas–solid measurements the relatively relevant non-linearity related to power concentration in doped chip heater in LCM 2524 induces increased uncertainties in comparison with chip NCM 9924. The introduction of Al-heater increases the reliability of the device.

From the comparison of laser sensitivity positional effects (S=$S(x, y)$ in relative scale) and the sensitivity obtained from Al-heater, the local absolute sensitivity can be determined. For instance, the sensitivity value corresponding to 1 mm^2 in the center of silicon surface is close to 1.24 V W^{-1}, and the mean value for an area of 5.76 mm^2 corresponding to a squared frame of side 4 mm and 0.36 mm wide, as schematized in Fig. 7c, reduces to 1.04 V W^{-1}. It means, in the case of surface energy dissipation without z-coordinate effect, when the dissipation is x–y dependent some auxiliary hypothesis about x–y distribution are necessary.

Remark

The use of flat detectors always requires an *x*–*y* positional analysis. When the dissipation is realized in a shell situated over the sensor, a complementary *z*-coordinate analysis is completely necessary [10].

Acknowledgements

The work is carried out in the frame of a cooperative program centered on the accuracy analysis of miniaturized calorimeters. The integrated action HA 2003-0034 (MCT-Spain) and D/03/39344 (Germany) between Freiberg and Barcelona groups are acknowledged.

References

1 W. Göpel, Sensors and Actuators B, 52 (1998) 125.
2 B. A. Snopok and I. V. Kruglenko, Thin Solid Films, 418 (2002) 21.
3 M. Bendahan, C. Jacolin, P. Lauque, J.-L. Seguin and P. Knauth, J. Phys. Chem. B, 105 (2001) 8327.
4 P. Lauque, M. Bendahan, J.-L. Seguin, K. An Ngo and P. Knauth, Anal. Chim. Acta, 515 (2004) 279.
5 J. Lerchner, D. Caspary and G. Wolf, Proc. SENSOR 97, A7.42, Nürnberg, 13–15 May, (1997) 225.
6 J. Lerchner, D. Caspary and G. Wolf, Sens. Actuators, B, 70 (2000) 57.
7 Liquid Microcalorimeter by Xensor Integration, Delft, The Netherlands (website:www.xensor.nl).
8 V. Torra, C. Auguet, J. Lerchner, P. Marinelli and H. Tachoire, J. Therm. Anal. Cal., 66 (2001) 255.
9 C. Auguet, F. Martorell, F. Moll and V. Torra, J. Therm. Anal. Cal., 70 (2002) 277.
10 C. Auguet, J. Lerchner, V. Torra and G. Wolf, J. Therm. Anal. Cal., 71 (2003) 407.
11 C. Auguet, J. Lerchner, P. Marinelli, F. Martorell, M. Rodriguez de Rivera, V. Torra and G. Wolf, J. Therm. Anal. Cal., 71 (2003) 951.
12 J. Pak, W. Qiu, M. Pyda, E. Nowak-Pyda and B. Wunderlich, J. Therm. Anal. Cal., 82 (2005) 565.
13 C. C Wang, S. A. Akbar and M. J. Madou, J. Electroceram., 2 (1998) 273.
14 O. Schäf, P. Lauque, J. L. Seguin, M. Eyraud and P. Knauth, Thin Solid Films, 389 (2001) 5.
15 M. Bendahan, P. Lauque, C. Lambert-Mauriat, H. Carchano and J.-L. Seguin, Sens. Actuators B, 84 (2002) 6.
16 M. Bendahan, P. Lauque, J.-L. Seguin, K. Aguir and P. Knauth, Sens. Actuators, B, 95 (2003) 170.
17 D. Caspary, M. Schröpfer, J. Lerchner and G. Wolf, Thermochim. Acta, 337 (1999) 57.
18 J. Lerchner, R. Kirchner, J. Seidel, D. Waehlisch and G. Wolf, Thermochim. Acta, 415 (2004) 27.
19 BPW 34 Datasheet, OSRAM Opto Semiconductors GmbH.
20 J. Lerchner, G. Wolf, C. Auguet and V. Torra, Thermochim. Acta, 382 (2002) 65.

Received: July 25, 2005
Accepted: March 23, 2006
OnlineFirst: August 11, 2006

DOI: 10.1007/s10973-005-7255-x